Supporting Information

for *Adv. Sci.*, DOI: 10.1002/advs.201600189

Visible and Near-Infrared Photothermal Catalyzed Hydrogenation of Gaseous CO_2 over Nanostructured $Pd@Nb_2O_5$

*Jia Jia, Paul G. O'Brien, Le He, Qiao Qiao, Laura M. Reyes, Timothy E. Burrow, Yuchan Dong, Kristine Liao, Maria Varela, Stephen J. Pennycook, Mohamad Hmadeh, Amr S. Helmy, Nazir P. Kherani, Doug D. Perovic, and Geoffrey A. Ozin**

Supporting Information

DOI: 10.1002/advs.201600189

Title: Visible and Near Infrared Photothermal Catalyzed Hydrogenation of Gaseous CO_2 over Nanostructured Pd@Nb_2O_5

*Jia Jia,[†] Paul G. O'Brien,[†] Le He, Qiao Qiao, Teng Fei, Laura M. Reyes, Timothy E. Burrow, Yuchan Dong, Kristine Liao, Maria Varela, Stephen J. Pennycook, Mohamad Hmadeh, Amr S. Helmy, Nazir P. Kherani, Doug D. Perovic, and Geoffrey A. Ozin **

Figure S1 (a) HAADF image of the $Nb_3O_7(OH)$ nanorods at low magnification. (b) HAADF image taken from a nanorod in its [001] direction. The preferred growth direction (longitudinal) of the nanorod is [010]. (c) FFT of (b) showing (200), (110) and (020) spots. (d) Atomic model indicated by the red rectangle in (b), where the dotted blue rectangle indicates a $Nb_3O_7(OH)$ unit cell.

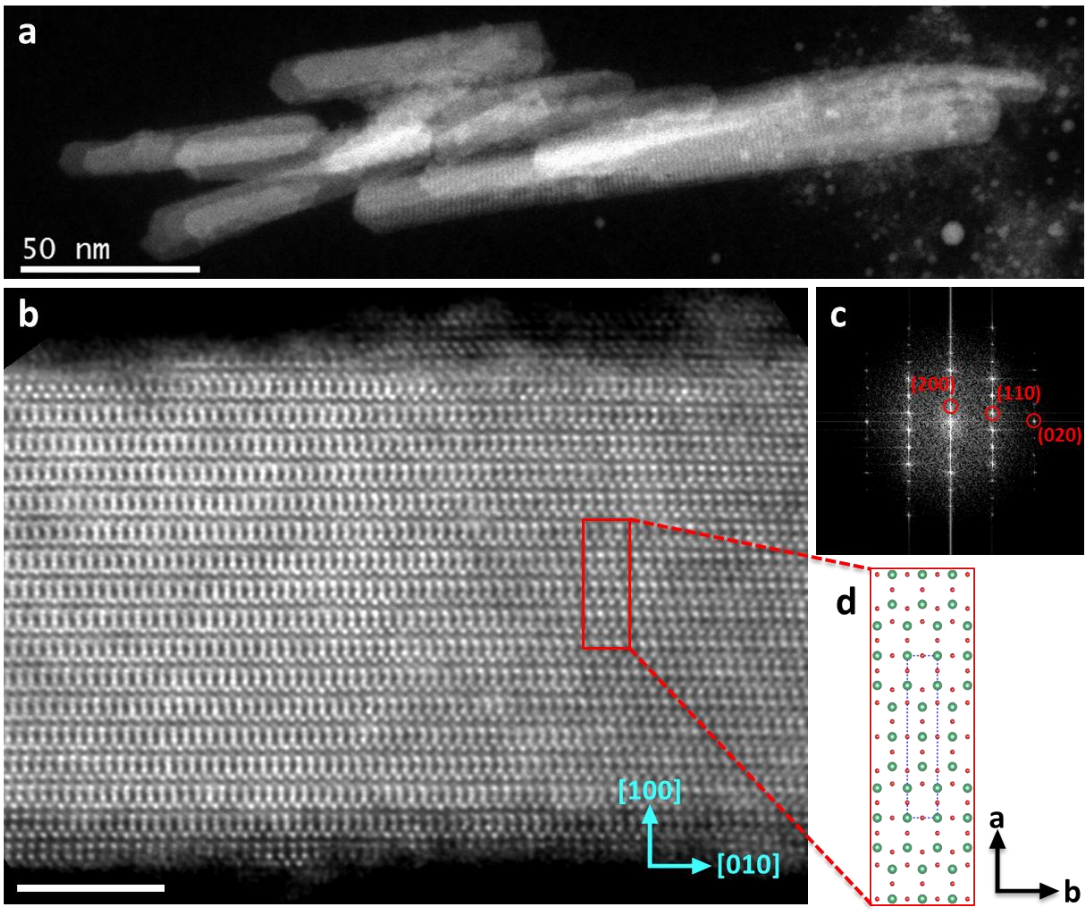

Figure S2. Powder X-ray diffraction patterns of Nb_2O_5, $Nb_3O_7(OH)$, 0.5% Pd@Nb_2O_5 (after pre-treatment) and 0.5% Pd@$Nb_3O_7(OH)$ (before pre-treatment).

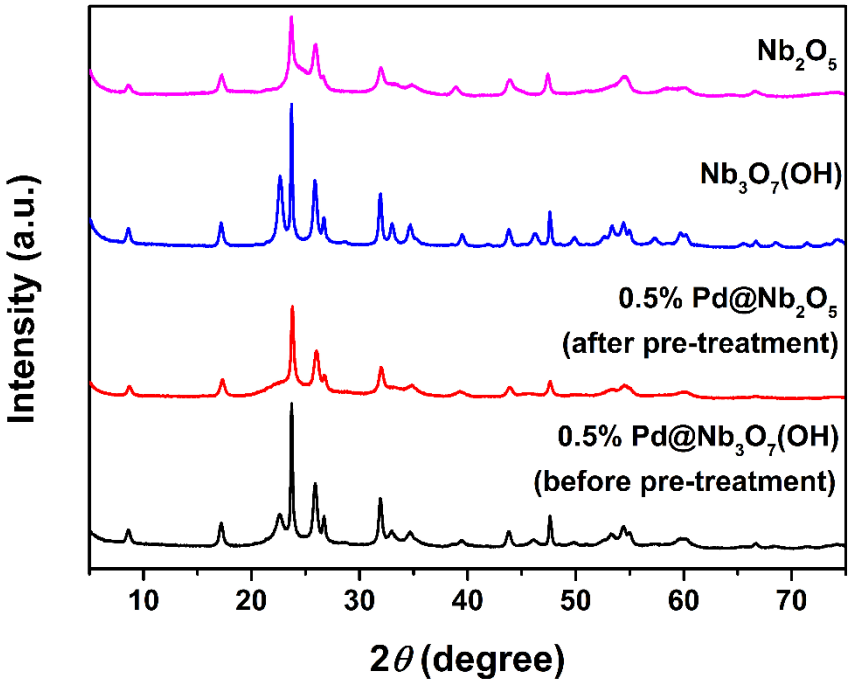

Figure S3. TEM images of (a) $Nb_3O_7(OH)$ nanorods and (b) Nb_2O_5 nanorods.

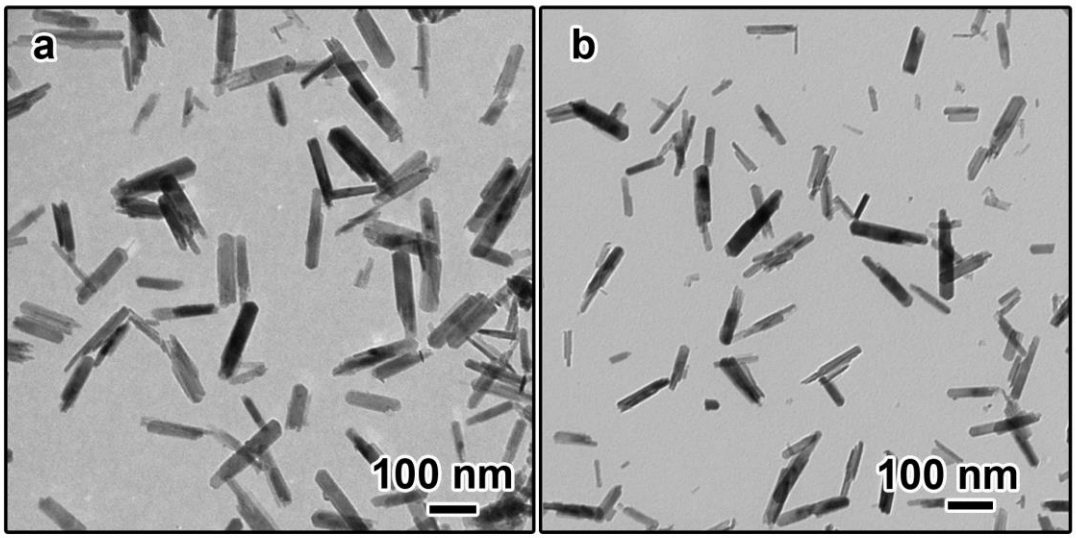

Figure S4. High resolution XPS spectra of the (a) Nb3d, (b) O1s and (c, d) Pd3d regions taken on Nb_2O_5, Pd@Nb_2O_5, 0.5% Pd@Nb_2O_5 and 1% Pd@Nb_2O_5, respectively.

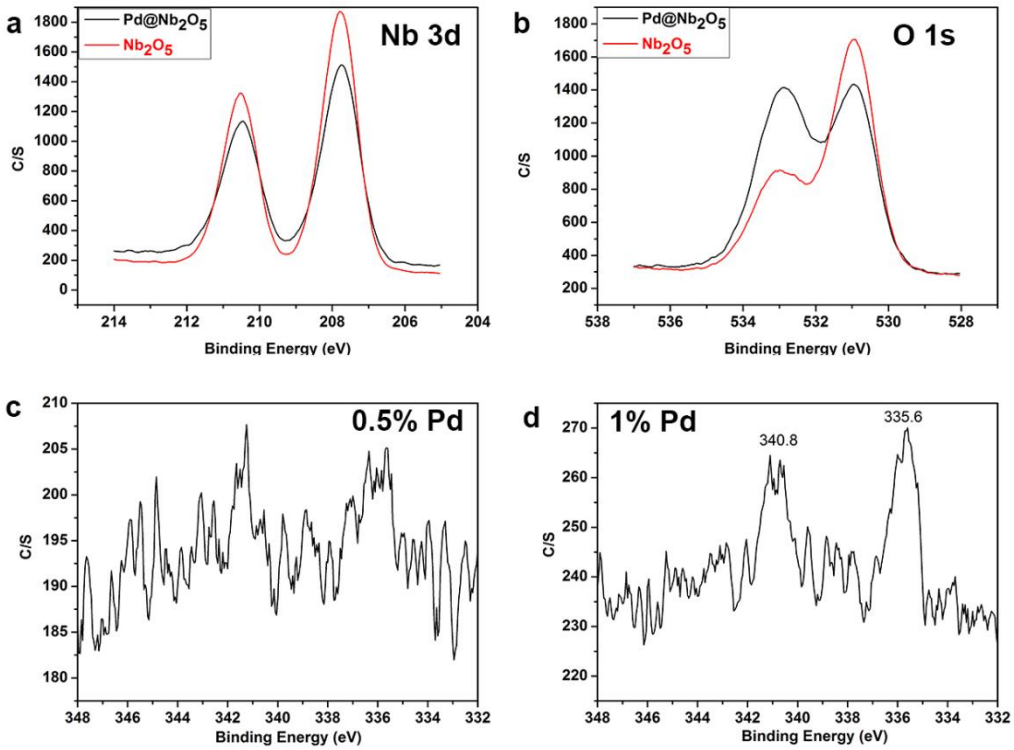

Figure S5. Estimation of the electronic band gap of Nb_2O_5. By using a modified Kubelka-Munk function, $(F(R)*h\nu)^n$ is plotted as a function of photon energy for Nb_2O_5 where $F(R) = (1-R)^2/2R$. Here R is the diffuse reflectance of the films loaded onto the borosilicate sample supports and n was set to 2 for Nb_2O_5. The linear portion of the plot was extrapolated and its intercept with the abscissa is considered to be the band-gap.

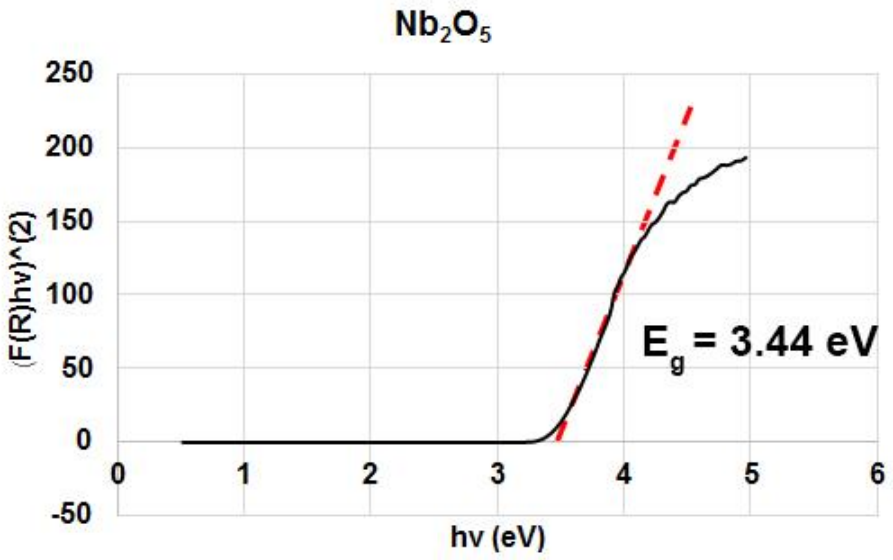

Figure S6. XPS Spectra of Nb_2O_5 (a) secondary electron cut-off region. (b) Valence band region (3.3 eV is relative to the work function.)

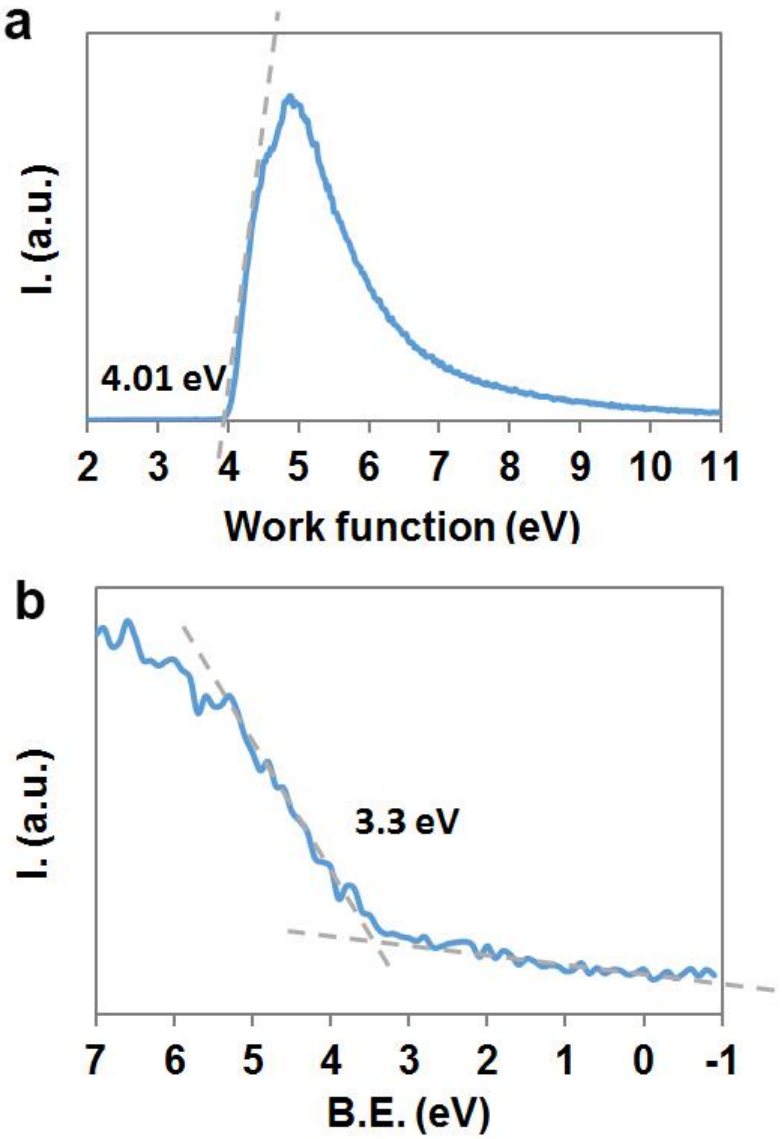

Figure S7. Mass spectrometry of photo-thermally generated ^{13}CO from $^{13}CO_2$. The 28 AMU mass fragment peak at approximately 1.32 min corresponds to N_2 and the 29 AMU mass fragment peak at approximately 1.345 min corresponds to ^{13}CO. The fact that there is no peak in the vicinity of 1.345 min retention time for the 28 AMU curve shows that there is no ^{12}CO in the products that could have been generated from sources of adventitious ^{12}C.

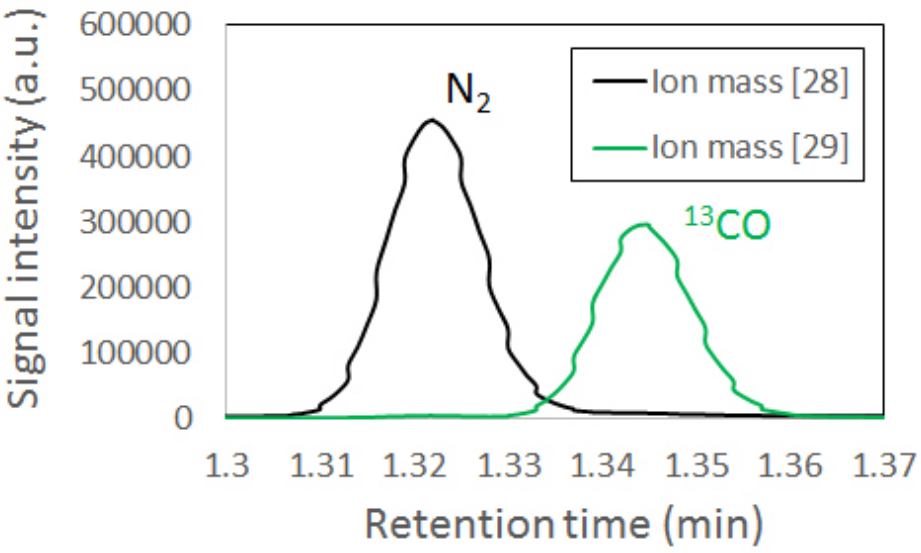

Figure S8. TEM image of Pd@Nb_2O_5 after gas-phase catalytic testing.

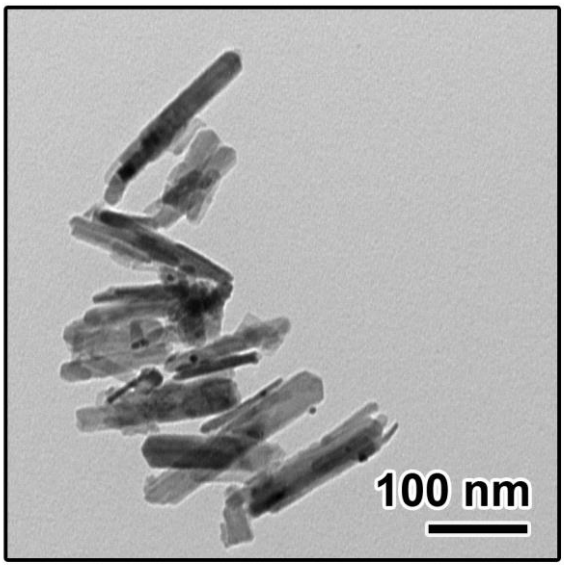

Figure S9. CO production rate from CO_2 in the presence and absence of H_2 over $Pd@Nb_2O_5$.

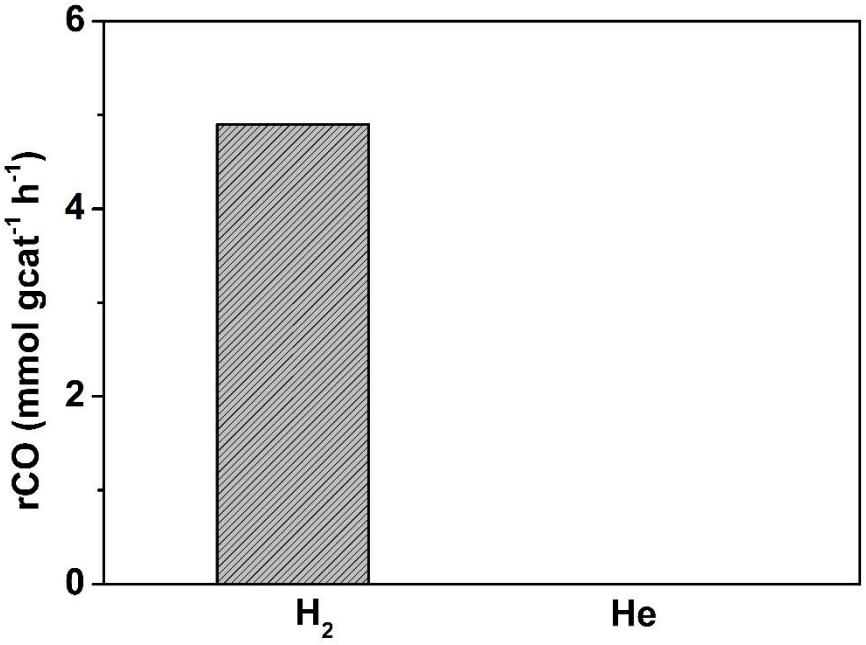

Figure S10. Thermogravimetric analysis (TGA) and differential thermogravimetric analysis of the fresh catalyst and used catalyst after catalytic reaction tests of 40 h

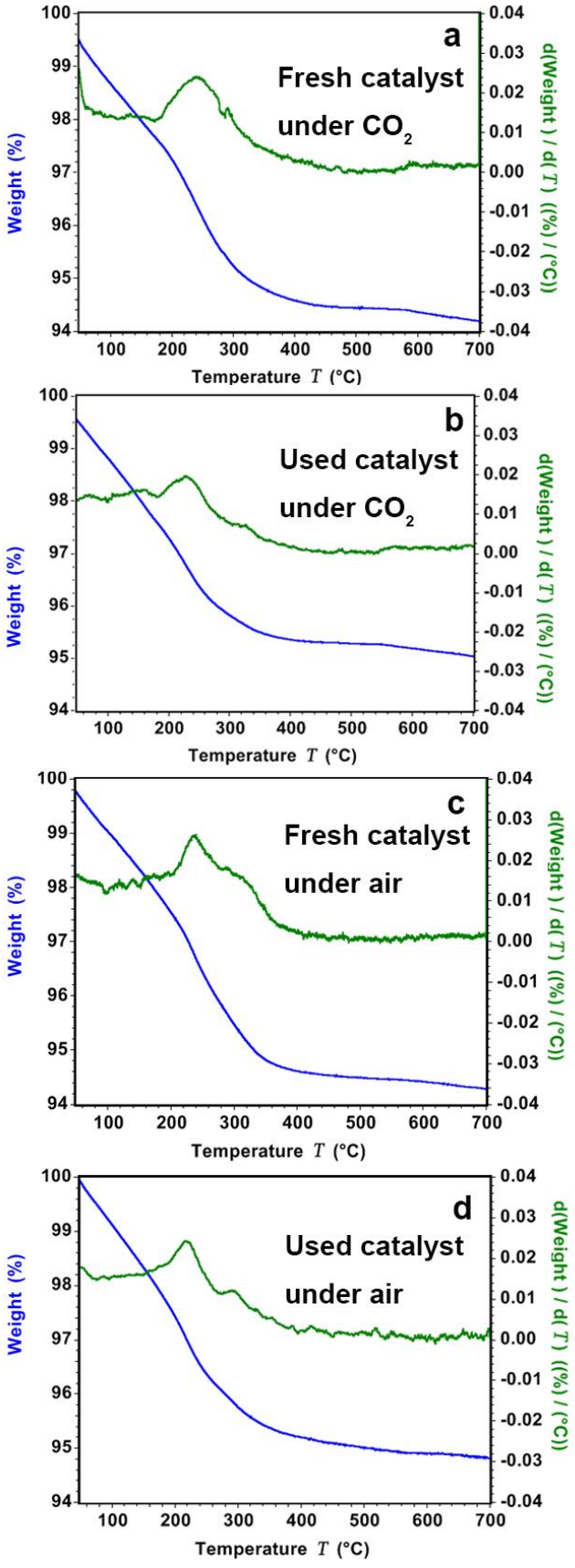

Figure S11. Dependence of the Raman frequency from 100 cm^{-1} to 1500 cm^{-1} for νNb=O stretching vibrations of a) $Pd@Nb_2O_5$ and b) Nb_2O_5 nanorods at different power levels.

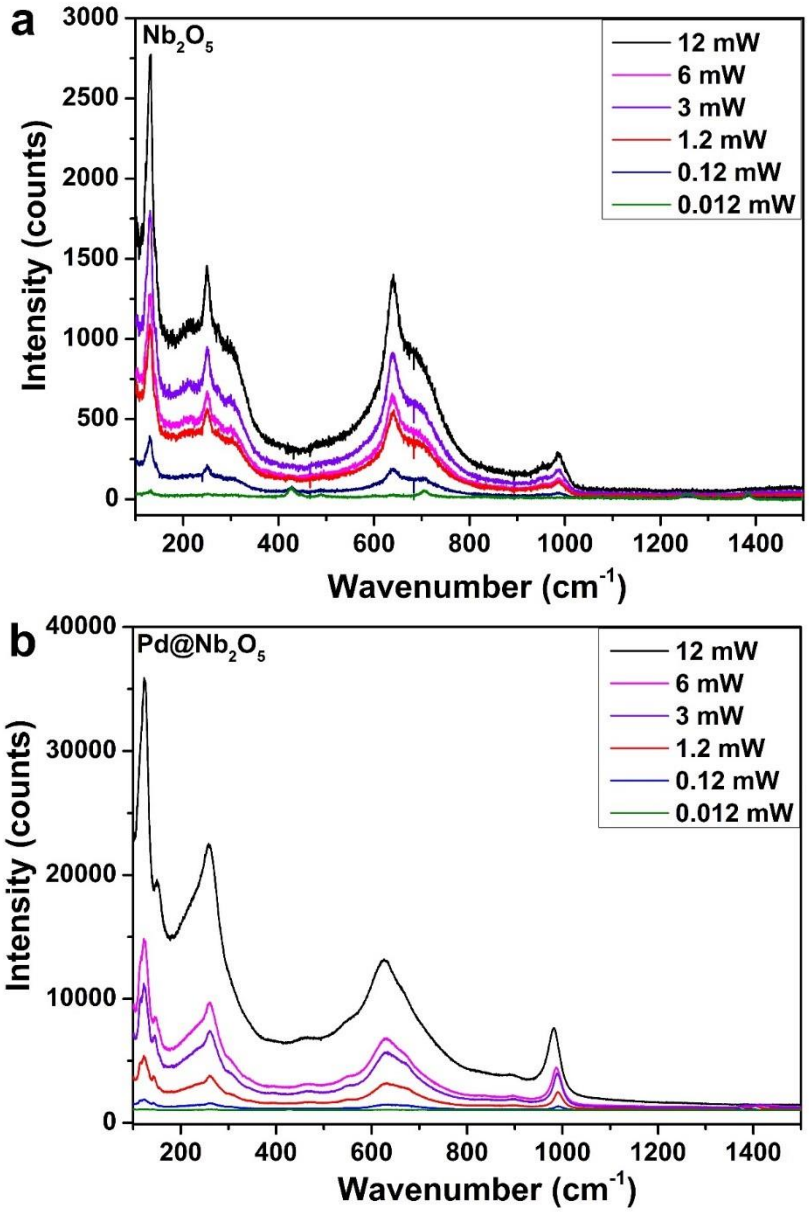

Figure S12. Selected wavelength Stokes and anti-Stokes Raman spectra between 500 cm^{-1} and 900 cm^{-1} with representative deconvolution of the spectra analyzed by LabSpec software for a) Pd@Nb_2O_5 Stokes spectra; b) Pd@Nb_2O_5 anti-Stokes spectra; c) Nb_2O_5 Stokes spectra and d) Nb_2O_5 anti-Stokes spectra.

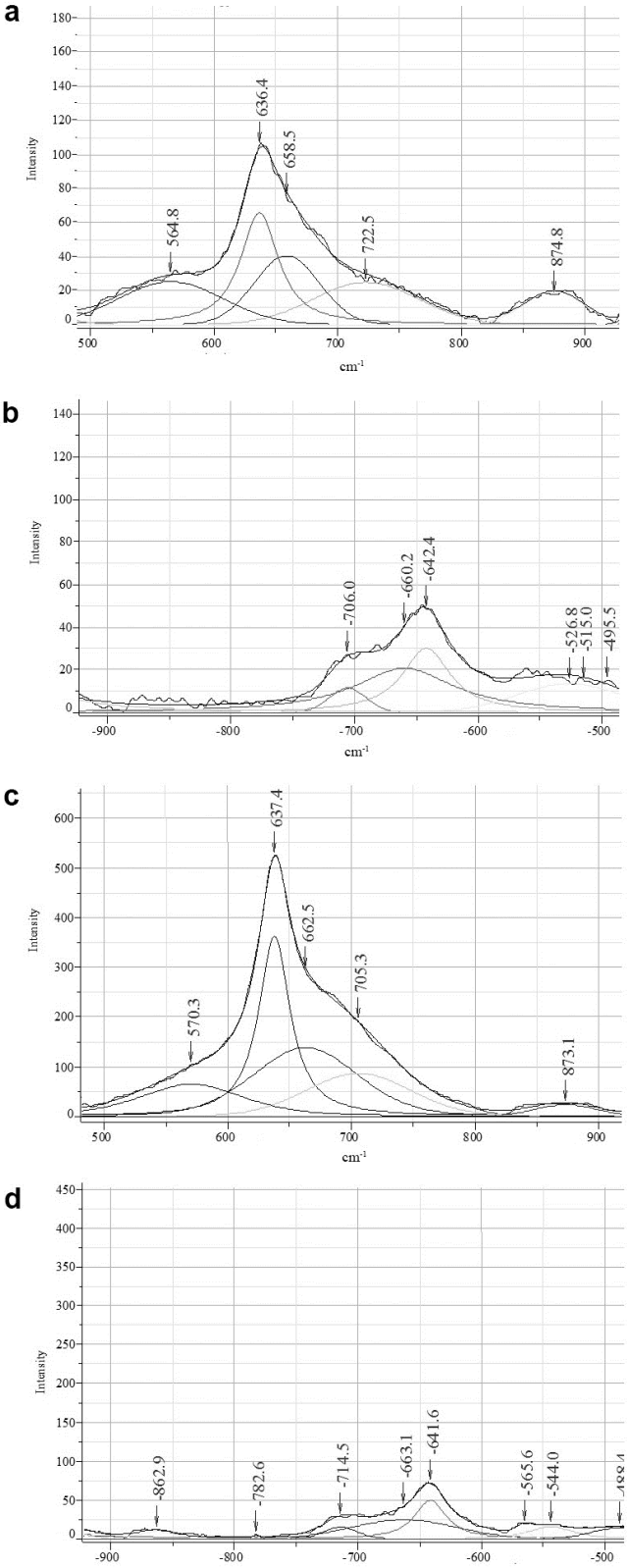

Figure S13. EPR spectra of Nb_2O_5 before (black) and after (red) being illuminated under a 300 W Xe lamp for 2 hours, recorded at 20 K.

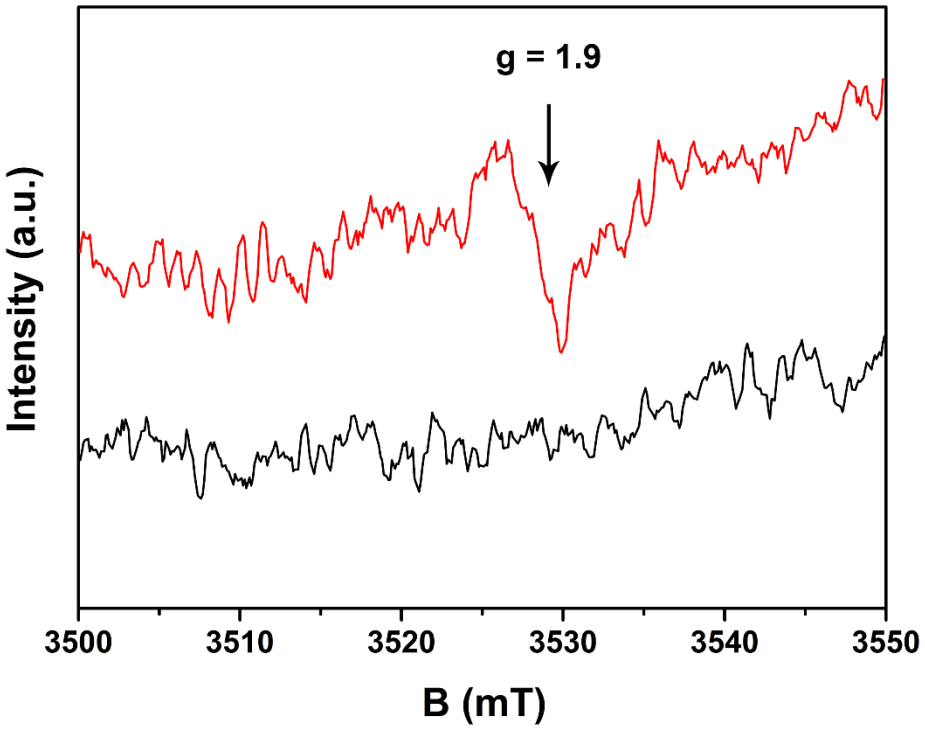

Figure S14. The photoreactor temperature as a function of time over the duration of a photothermal test. The temperature inside the reactor is 49.7 °C at the 3 h point of the test. The temperature of the sample is much greater than that of the reactor due to the photothermal effect.

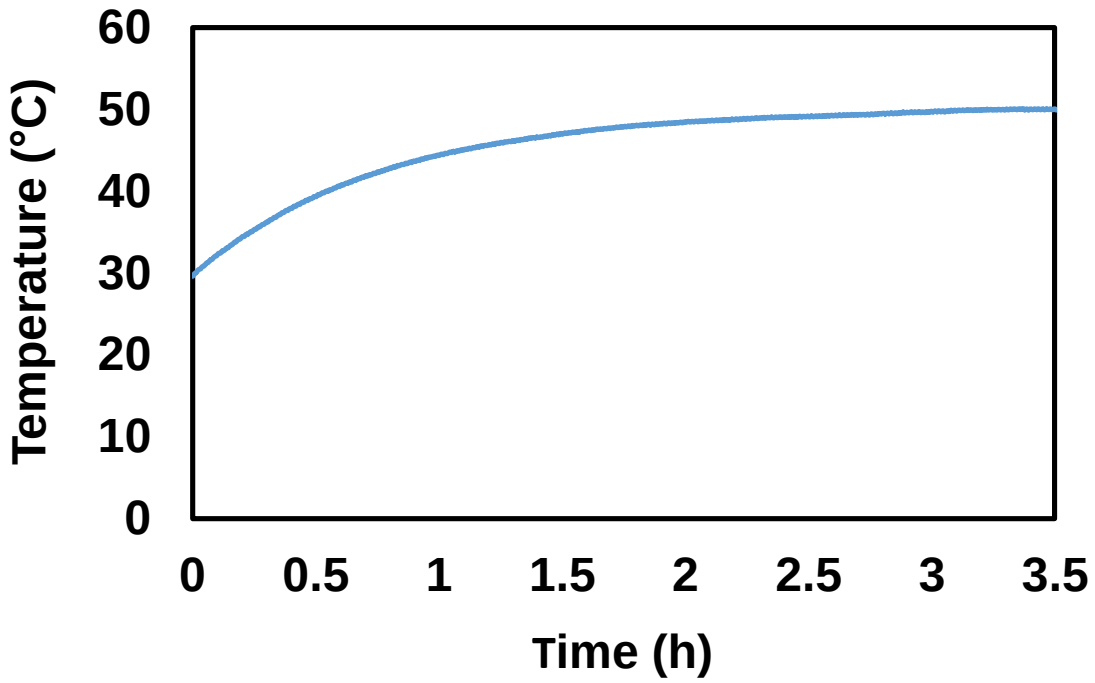

Table S1. Estimation of reaction temperatures over $Pd@Nb_2O_5$ under irradiation from the 300 W Xe lamp using different cut-off filters for batch reactions A through F and without any filter at different light intensities for batch reactions I through V.

Sample	**k (mmol $g^{-1}h^{-1}$)**	**T(K estimated)**	**T(°C estimated)**
A(I)	4.9	470	197
B	3.5	462	190
C	1.8	447	174
D	1.1	436	163
E	0.78	430	157
F	0.41	417	144
II	3.3	461	189
III	0.95	434	161
IV	0.63	426	153
V	0.56	423	150

Table S2. Summary of the Raman band frequency for the ν(Nb=O) stretching vibrations of $Pd@Nb_2O_5$ and Nb_2O_5 at different power levels using a 633 nm laser. Temperature estimation was performed using the slope of the dependence of the Raman band shift on temperature in prior work.[1]

Power levels (mW)	**$Pd@Nb_2O_5$**			**Nb_2O_5**		
	Peak position (cm^{-1})	**Band shift (cm^{-1})**	**Estimated T (K)**	**Peak position (cm^{-1})**	**Band shift (cm^{-1})**	**Estimated T (K)**
12	981.5	-10.5	777	985.7	-1.5	368
6	986.9	-5.1	531	986.3	-0.9	341
3	989.3	-2.7	422	986.6	-0.6	327
1.2	990.5	-1.5	368	986.9	-0.3	314
0.12	991.1	-0.9	341	987.2	0	300
0.012	992.0	0	300	987.2	0	300

Table S3. Estimation of the temperature of $Pd@Nb_2O_5$ and Nb_2O_5 under the power level of 24 mW using a laser pump wavelength of 785 nm. The signals of the Raman Stokes and anti-Stokes scattering at around 640 cm^{-1} are obtained from the deconvolution of the spectra by LabSpec software, as shown in Figure S11. The estimation of temperatures is calculated using the ratio of Stokes signals to anti-Stokes signals and the band position of the Raman modes.

Sample	**Stokes signal (S) area**	**anti-Stokes (AS) signal area**	**S/AS Ratio**	**ω (cm^{-1})**	**T (K)**
$Pd@Nb_2O_5$	65.96	30.18	2.185	636.44	776
Nb_2O_5	362.91	49.77	7.291	637.42	385

Reference

[1] S. Xie, E. Iglesia, A. T. Bell, *J. Phys. Chem. B* **2001**, 105, 5144.